CRYSTAL GROWTH & DESIGN

Article

pubs.acs.org/crystal

Series of Organic–Inorganic Hybrid Rare Earth Derivatives Based on $[MnV_{13}O_{38}]^{7-}$ Polyoxoanion: Syntheses, Structures, and Magnetic and Electrochemical Properties

Published as part of the Crystal Growth & Design virtual special issue IYCr 2014 - Celebrating the International Year of Crystallography

Ding Liu,[†] Ying Lu,*[,†] Hua-Qiao Tan,[‡] Ting-Ting Wang,[†] and En-Bo Wang*[,†]

[†]Key Laboratory of Polyoxometalate Science of Ministry of Education, Department of Chemistry, Northeast Normal University, Ren Min Street No. 5268, Changchun, Jilin 130024, P. R. China

[‡]State Key Laboratory of Luminescence and Applications, Changchun Institute of Optics, Fine Mechanics and Physics, Chinese Academy of Sciences, 3888 East Nanhu Road, Changchun 130033, P. R. China

Supporting Information

ABSTRACT: A family of polyoxometalate compounds based on 1:13 polyoxoanions $[MnV_{13}O_{38}]^{7-}$, organic molecules, and lanthanide cations, $H[\{La_2(DMF)_5(H_2O)_4\}\{MnV_{13}O_{38}\}]\cdot DMF\cdot 5H_2O$ (**1**), $H[\{Ce_2(DMF)_2(H_2O)_7\}\{MnV_{13}O_{38}\}]\cdot 0.5DMF\cdot 5.5H_2O$ (**2**), $H_2[\{K(H_2O)_2\}_2\{Nd(DMF)(H_2O)_3\}\{MnV_{13}O_{38}\}]\cdot 5H_2O$ (**3**), $H[\{Ln_2(C_6H_5NO_2)_3(H_2O)_6\}\{[MnV_{13}O_{38}\}]\cdot C_6H_5NO_2\cdot 10H_2O$ (Ln = La **4**, Ce **5**), and $H_{2.5}[\{Pr(C_6H_5NO_2)(H_2O)_{3.5}\}\{Pr_{0.5}(H_2O)_2\}\{MnV_{13}O_{38}\}]\cdot 0.5C_6H_5NO_2\cdot 10H_2O$ (**6**) (DMF = *N*,*N*-dimethylformamide; $C_6H_5NO_2$ = isonicotinic acid), have been obtained utilizing a conventional method of aqueous solution and further characterized by elemental analysis, IR spectrum, UV spectrum, thermogravimetric analysis, and single-crystal X-ray diffraction. Compounds **1** and **2** exhibit a one-dimensional extended chain structure constructed by $[MnV_{13}O_{38}]^{7-}$ and lanthanide-organic coordination linkage, while compound **3** reveals three-dimensional (3D) open framework formed by polyoxoanion-lanthanide chains and potassium cations. Compounds **4**–**6** exhibit 3D supramolecular framework architectures based on $[MnV_{13}O_{38}]^{7-}$ polyoxoanions and lanthanide-organic coordination units. These compounds represent the first examples of extended organic–inorganic hybrids built up by $[MnV_{13}O_{38}]^{7-}$ building blocks and rare earth cations. The influences of the lanthanide contraction effect on the structural alterations from **1** to **3** and from **4** to **6** have been disscussed. The electrochemical and electrocatalytic properties for compounds **1**–**6** have been studied. Magnetic studies indicate that antiferromagnetic interactions exist in compounds **1**–**6**.

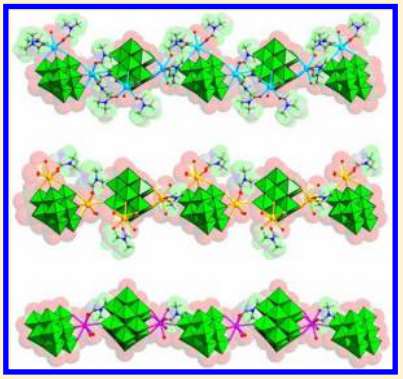

INTRODUCTION

Crystalline organic–inorganic hybrids are a family of complexes that combine organic moieties, inorganic units and metal nodes in an integrated framework through organizing structures by grafting, intercalation and self-assembly.[1] Such hybrids exhibit structural variability and intriguing applications in the fields of electrical conductivity, catalysis, selective adsorption, photochemistry, and magnetism.[2]

Polyoxometalates (POMs), as a characteristic class of discrete-anionic metal-oxo clusters, have recently attracted extensive interests owing to their abundant topologies and multiple functionality, rendering them active candidates in solid-state materials chemistry.[3] Especially, decorating POMs by attaching organic molecules offers a significant synthetic method for the preparation of functional POM crystalline materials. To date, diverse POM-based inorganic–organic hybrids have been synthesized and characterized.[4] The intrinsic quality of both the organic and inorganic components have a significant influence on the structures and properties of the formed hybrid materials.[5] Up to now, classic POM building blocks such as Keggin, Anderson, Dawson-type heteropolyoxoanion and isopolyoxoanion units have been chosen to be applied in the construction of POM-based hybrids.[6] However, it is still a great challenge to design and synthesize organic functionalized POMs with new POM species. Generally, the methods of architectural design and synthesis of POM-based hybrids are almost semiempirical, mainly depending on the experimental phenomena and intuition of construction processes, which are indirectly influenced by concentration, pH, temperature, ionic strength, etc. Owing to the little directional information, it is difficult to predict the relevant steric configuration between the POM clusters and the organic units.[7] Consequently, great efforts have been devoted to control

Received: June 30, 2014
Revised: November 3, 2014
Published: December 3, 2014

the assembly processes for offering elaborate structures from simple precursors.

POMs can act as inorganic electron-donor ligands to connect transition metals or lanthanide cations at specific sites and incorporate organic moieties to exhibit novel packing sublattice in the hybrid materials.[8] Among the large family of POMs, the unusual $[MnV_{13}O_{38}]^{7-}$ (abbreviated as $\{MnV_{13}\}$) polyoxoanion caught our attention.[9] $[MnV_{13}O_{38}]^{7-}$ anions are easy to combine with electrophilic transition-metal or rare-earth-metal linkers because as polyoxovanadate it possesses higher surface-oxygen charge density in comparison to polyoxomolybdate and polyoxotungtate.[10] In addition, $[MnV_{13}O_{38}]^{7-}$ is a kind of functional POM, which shows catalytic oxidation performance in some organic reactions, and its antibacterial/antitumor medical activities have been studied.[11] Our previous work has reported pure inorganic porous material constructed from $\{MnV_{13}\}$ polyoxoanion with rare earth cations as connections, while $\{MnV_{13}\}$-based higher dimensional inorganic−organic compounds remain rarely exploited.[12]

Therefore, the exploration and controlled synthesis of novel inorganic−organic hybrids composed of $\{MnV_{13}\}$ clusters and lanthanide-organic subunits is our pursuit. N,N-Dimethylformamide and isonicotinic acid ligands were selected herein as the agent source not only because of the synergistic effects between the rare earth cations and the oxide-containing donor, but also the small steric size of the ligands facilitates the connectivity of the adjacent $\{MnV_{13}\}$ polyoxoanions and avoids aggregation. Furthermore, on the basis of the different nature of small ligands DMF and carboxylic acids, several different architectures were isolated: $H[\{La_2(DMF)_5(H_2O)_4\}\{MnV_{13}O_{38}\}]\cdot DMF\cdot 5H_2O$ (**1**), $H[\{Ce_2(DMF)_2(H_2O)_7\}\{MnV_{13}O_{38}\}]\cdot 0.5DMF\cdot 5.5H_2O$ (**2**), $H_2[\{K(H_2O)_2\}_2\{Nd(DMF)(H_2O)_3\}\{MnV_{13}O_{38}\}]\cdot 5H_2O$ (**3**), $H[\{La_2(C_6H_5NO_2)_3(H_2O)_6\}\{[MnV_{13}O_{38}\}]\cdot C_6H_5NO_2\cdot 10H_2O$ (**4**), $H[\{Ce_2(C_6H_5NO_2)_3(H_2O)_6\}\{MnV_{13}O_{38}\}]\cdot C_6H_5NO_2\cdot 10H_2O$ (**5**), and $H_{2.5}[\{Pr(C_6H_5NO_2)(H_2O)_{3.5}\}\{Pr_{0.5}(H_2O)_2\}\{MnV_{13}O_{38}\}]\cdot 0.5C_6H_5NO_2\cdot 10H_2O$ (**6**). The electrochemical and magnetic properties of the complexes were also studied. These compounds represent the first examples of extended organic−inorganic hybrids based on $[MnV_{13}O_{38}]^{7-}$ building blocks and lanthanide cations.

EXPERIMENTAL SECTION

Materials and Methods. All raw materials were commercially purchased and used without further purification. $K_7[MnV_{13}O_{38}]\cdot 18H_2O$ was synthesized according to the literature and characterized by IR spectrum.[10a] IR spectra were recorded in the range of 400−4000 cm^{-1} on an Alpha Centaurt FT/IR spectrophotometer with pressed KBr pellets. Elemental analyses (H, N, and C) were performed on a PerkinElmer 2400 CHN elemental analyzer; Mn, K, V, La, Ce, Pr, and Nd were analyzed on a PLASMA-SPEC (I) ICP atomic emission spectrometer. Thermogravimetric (TG) analyses were analyzed on a Perkin−Elmer TGA7 instrument in flowing N_2 with a heating rate of 10 °C·min^{-1}. UV−vis absorption spectra were obtained using a 725 PC UV−vis spectrophotometer. The electrochemical measurement was carried out on a CHI 660 electrochemical workstation. All measurements were performed at room temperature. Variable-temperature magnetic susceptibility data were obtained on a SQUID magnetometer (Quantum Design, MPMS-7) in the temperature range of 2−300 K with an applied field of 0.1 T.

Synthesis of ***1****.* $K_7[MnV_{13}O_{38}]\cdot 18H_2O$ (0.5 g, 0.26 mmol) was dissolved in 15 mL of distilled water, and then $LaCl_3$ (0.25 g, 1.0 mmol) and 5 mL of DMF were added into the above solution with vigorously stirring. The mixed solution was heated at 40 °C for 4 h with stirring. Then the mixture was cooled to room temperature. The filtrate was kept for 2 weeks at ambient conditions, and then orange block crystals of **1** were obtained (yield: 43% based on $K_7[MnV_{13}O_{38}]\cdot 18H_2O$). Calcd for **1**: C, 9.81; H, 2.79; N, 3.81; La, 12.60; Mn, 2.50 and V, 30.04%. Found: C, 9.35; H, 2.61; N, 3.59; La, 11.76; Mn, 2.83 and V, 30.27%. IR (KBr pellet) for **1**: ν/cm^{-1} = 3422 (m), 2930 (w), 1645 (s), 1495 (w), 1434 (m), 1382 (s), 1249 (w), 1110 (m), 978 (s), 937 (s), 828 (m), 652 (s), 594 (s), 441 (m).

Synthesis of ***2****.* The preparation process of **2** was similar to **1** except that $Ce(NO_3)_3\cdot 6H_2O$ (0.43 g, 1.0 mmol) was adopted instead of $LaCl_3$. Brown crystals of **2** were harvested after 1 week (yield: 35% based on $K_7[MnV_{13}O_{38}]\cdot 18H_2O$). Calcd for 2: C, 4.47; H, 2.13; N, 1.74; Ce, 13.92; Mn, 2.73 and V, 32.89%. Found: C, 4.75; H, 2.61; N, 1.35; Ce, 11.79; Mn, 3.12 and V, 32.57%. IR (KBr pellet) for **2**: ν/cm^{-1} = 3421 (m), 2930 (w), 1645 (s), 1495 (w), 1434 (m), 1382 (s), 1249 (w), 1110 (m), 977 (s), 924 (s), 829 (m), 652 (s), 594 (s), 441 (m).

Synthesis of ***3****.* The synthetic method of compound **3** was identical to the preparation of **1** except using $Nd(NO_3)_3$ (0.33 g, 1.0 mmol) instead of $LaCl_3$. Brown crystals of **3** were havested after 3 weeks (yield: 37% based on $K_7[MnV_{13}O_{38}]\cdot 18H_2O$). Calcd for **3**: C, 1.96; H, 1.81; N, 0.76; K, 4.25; Nd, 7.84; Mn, 2.99 and V, 36.01%. Found: C, 1.57; H, 1.73; N, 0.82; K, 4.31; Nd, 8.04, Mn, 2.75 and V, 35.57%. IR (KBr pellet) for 3: ν/cm^{-1} = 3418 (m), 1648 (s), 1493 (w), 1432 (m), 1382 (m), 1248 (w), 1113 (m), 975 (s), 937 (s), 823 (m), 659 (s), 597 (s), 438 (m).

Synthesis of ***4****.* $K_7[MnV_{13}O_{38}]\cdot 18H_2O$ (0.5 g, 0.26 mmol) was dissolved in 25 mL of hot water, and then $LaCl_3$ (0.25 g, 1.0 mmol) and isonicotinic acid (2.4 g, 0.30 mmol) were added to the above solution with stirring successively. The pH value of the mixed solution was carefully adjusted to 2.7 with 2 M dilute H_2SO_4 solution. Afterward, the mixture was heated at 45 °C for 3 h with stirring, and then filtered. The filtrate was kept at room temperature, and orange crystals of **4** were afforded after 1 week (yield: 53% based on $K_7[MnV_{13}O_{38}]\cdot 18H_2O$). Calcd for **4**: C, 12.09; H, 2.24; N, 2.35; La, 11.65; Mn, 2.30 and V, 27.77%. Found: C, 12.63; H, 1.85; N, 1.97; La, 12.15, Mn, 2.61 and V, 28.52%. IR (KBr pellet) for **4**: ν/cm^{-1} = 3354 (m), 3074 (m), 1727 (w), 1589 (s), 1385 (s), 1283 (w), 1246 (w), 979 (m), 942 (s), 861 (w), 825 (m), 762 (m), 721 (w), 653 (m), 596 (m), 441 (m).

Synthesis of ***5****.* A similar method was followed to prepare **5** except $Ce(NO_3)_3\cdot 6H_2O$ (0.43 g, 1.0 mmol) was added. Orange block crystals of **5** were isolated after 5 days (yield: 42% based on $K_7[MnV_{13}O_{38}]\cdot 18H_2O$). Calcd for **5**: C, 12.07; H, 2.24; N, 2.35; Ce, 11.74; Mn, 2.30 and V, 27.74%. Found: C, 12.47; H, 2.43; N, 1.92; Ce, 11.39, Mn, 2.16 and V, 26.79%. IR (KBr pellet) for 5: ν/cm^{-1} = 3387 (m), 3073 (m), 1725 (w), 1589 (s), 1385 (s), 1283 (w), 1247 (w), 978 (m), 940 (s), 826 (w), 760 (m), 721 (w), 652 (m), 597 (m), 441 (m).

Synthesis of ***6****.* Compound **6** was prepared similarly to **4**, with $PrCl_3$ (0.25 g, 1.0 mmol) instead of $LaCl_3$. Light orange block crystals were obtained from the solution after 1 week (yield: 40% based on $K_7[MnV_{13}O_{38}]\cdot 18H_2O$). Calcd for **6**: C, 5.40; H, 2.06; N, 1.05; Pr, 10.55; Mn, 2.74 and V, 33.06%. Found: C, 4.93; H, 1.85; N, 0.95; Pr, 1 0.07, Mn, 2.83 and V, 32.57%. IR (KBr pellet) for **6**: ν/cm^{-1} = 3363 (m), 1725 (w), 1589 (s), 1384 (s), 1283 (w), 1245 (w), 1134 (m), 974 (s), 940 (s), 824 (w), 762 (m), 652 (m), 593 (m), 439 (m).

X-ray Crystallography. Single-crystal X-ray crystallographic data were collected on a Rigaku R-AXIS RAPID IP diffractometer equipped with a normal focus 18 kW sealed tube X-ray source (MoKα radiation, λ = 0.71073 Å) operating at 50 kV and 200 mA at T = 293 K. The crystal data of **1**−**6** were solved by direct methods and refined by a full-matrix least-squares method on F^2 using the *SHELXL-97* crystallographic software package.[13] The final residuals (R_1 = 0.0785, wR_2 = 0.2068 for **2**; R_1 = 0.0893, wR_2 = 0.1948 for **6**) are relatively large for **2** and **6** due to the limited data-quality of the single crystals; however, the polyoxoanions and lanthanide-organic fragments in these structures are well behaved, and there are no unusual temperature factors or excursions of electron density in these regions of the structure. In addition, for compounds **1**−**6**, the hydrogen atoms attached to water molecules were not located and the hydrogen atoms attached to nitrogen atoms and carbon atoms were fixed in ideal

dx.doi.org/10.1021/cg500955d | *Cryst. Growth Des.* 2015, 15, 103−114

Table 1. Crystal Data and Structure Refinements for Compounds 1−6

compound	1	2	3	4	5	6
empirical formula	$C_{18}H_{61}N_6MnV_{13}La_2O_{53}$	$C_{7.5}H_{42.5}N_{2.5}MnV_{13}Ce_2O_{53}$	$C_3H_{33}NMnV_{13}K_2NdO_{51}$	$C_{24}H_{53}N_4MnV_{13}La_2O_{62}$	$C_{24}H_{53}N_4MnV_{13}Ce_2O_{62}$	$C_9H_{41}N_{1.5}MnV_{13}Pr_{1.5}O_{56.5}$
M_r	2204.71	2012.34	1838.90	2384.68	2387.10	2002.96
temperature (K)	296(2)	293(2)	293(2)	296(2)	293(2)	293(2)
crystal system	orthorhombic	triclinic	monoclinic	monoclinic	monoclinic	triclinic
space group	*Pbca*	$P\bar{1}$	$P2_1/n$	$P2_1/n$	$P2_1/n$	$P\bar{1}$
a/Å	23.711	14.379	12.619	13.042	13.021	12.959
b/Å	24.389	22.686	19.525	22.879	22.787	21.707
c/Å	25.303	23.782	21.983	22.220	22.153	21.853
α/°	90.00	89.45	90.00	90.00	90.00	86.36
β/°	90.00	80.52	95.07	97.35	97.44	83.99
γ/°	90.00	77.84	90.00	90.00	90.00	86.79
V/Å^3	14632.5	7477	5395	6576	6518	6094
Z	8	4	4	4	4	4
D_c/g cm^{-3}	2.002	1.788	2.264	2.409	2.433	2.183
F(000)	8584	3876	3552	4636	4644	3880
reflns collected/unique	71329/12873	53887/24475	39419/9469	32787/11561	47302/11434	43181/19838
R_{int}	0.0647	0.0528	0.0822	0.0291	0.1285	0.0783
GOF on F^2	0.994	1.024	1.033	1.040	1.034	0.914
R_1[a] $[I > 2\sigma(I)]$	0.0567	0.0785	0.0659	0.0295	0.0639	0.0893
wR_2[b]	0.1584	0.2068	0.1494	0.0773	0.1258	0.1948
largest residuals [e·Å^{-3}]	2.817/−1.125	2.971/−0.788	2.081/−1.047	0.849/−0.710	0.949/−0.950	2.272/−2.723

[a] $R_1 = \Sigma||F_o| - |F_c||/\Sigma|F_o|$. [b] $wR_2 = \Sigma[w(F_o^2 - F_c^2)^2]/\Sigma[w(F_o^2)^2]^{1/2}$.

positions. All the H atoms on water molecules were directly included in the molecular formula. A summary of the crystallographic data and structural determination for compounds **1**−**6** is provided in Table 1. Further details of the crystal structures can be obtained from the Fachinformationszentrum Karlsruhe, D-76344 Eggenstein−Leopoldshafen, Germany (the CCDC reference numbers are 1009719−1009724).

RESULTS AND DISCUSSION

Synthesis. *Synthesis.* We have investigated the reactivity of $[MnV_{13}O_{38}]^{7-}$ polyoxoanion and early/middle lanthanide cations with small organic ligands. Abundant parallel experiments demonstrate that concentration, pH, temperature and ratio of reagents are important synthetic factors for the isolation of **1**−**6**. The suitable temperature of the reactions is 40 °C. If the solution temperature is higher than 50 °C, a amount of brown MnO_2 precipitates were formed because the oxidation rate of Mn^{2+} was increased. Compounds **4**−**6** could only be isolated in the pH range from 2.5 to 3.0. When the reaction pH value was lower than 2.5, the products were unidentified polycrystals. If the pH value of the reaction exceeded 3.0, no crystalline phase was obtained as the hydrolysis of the lanthanide cation easily occurs at higher pH values. Compared with **4**−**6**, compounds **1**−**3** can be isolated over a relatively wide pH range. Experiments show that the products of these three compounds can be obtained in the pH range 2.3−3.5. Therefore, the experimental process should be regulated very carefully to generate the pure title crystals. Compounds **1**−**6** can be isolated by using a 1:4 $[MnV_{13}O_{38}]^{7-}/Ln^{3+}$ proportion, and the excess Ln^{3+} component is beneficial to obtain products in high yields. Compounds **1**−**6** possess different architectures, although they were prepared by the similar $[MnV_{13}O_{38}]^{7-}/Ln^{3+}$ ratio. In the syntheses of compounds **1**−**3**, *N*,*N*-dimethylformamide (DMF) plays a dual role because it can not only work as solvent but also provides ligand molecule. And the introduction of the isonicotinic acid molecule in the reaction system is critical for the isolation of **4**−**6**. To investigate the effect of different organic ligands on structural diversity, we attempted to replace DMF and isonicotinic acid with other organic molecules (dimethyl sulfoxide, proline, or alanine) with different size under the similar conditions and only obtained some amorphous precipitate. When we used *N*-methyl-2-pyrrolidone and nicotinic acid as ligands, the organic molecules acted as structure-directing agents in the $[MnV_{13}O_{38}]^{7-}/Ln^{3+}$ system and not link to the lanthanide cations. It can be concluded that the introduction of organic ligands may stabilize the Ln cations and prevent the high reactivity of lanthanide cations with polyoxoanions, and the size/coordination mode of the organic ligands plays a key factor in the construction of products. The target compounds **1**−**6** have been obtained through employing of lanthanide cations such as La^{3+}, Ce^{3+}, Nd^{3+}, and Pr^{3+}. Additionally, when other Ln cations (Eu, Gd, Sm, and Dy) replace those in **1**−**6** under the same conditions, to our regret, only some polycrystalline powders were obtained. Obviously, the systematic exploration of lanthanide $\{MnV_{13}\}$-organic complexes still remains a great challenge to us. Further work is in progress for exploiting the formation mechanism and the pertinent synthetic chemistry by using various ligands and different polyoxovanadate.

Structure Description. *Crystal Structure of 1.* Single-crystal X-ray diffraction analysis demonstrates that compound **1** crystallized in the orthorhombic space group P_{bca}. The fundamental structural unit of **1** was constructed of two crystallographically unique La atoms, one $\{MnV_{13}\}$ anion, five DMF ligands, one DMF solvent, and five lattice water molecules. As shown in Figure 1, the $\{MnV_{13}\}$ precursor is maintained in **1**. This polyoxoanion is composed of one Mn atom as octahedral central cavity surrounded by 13 edge-shared VO_6 octahedra (Figure S1, Supporting Information). There are four kinds of oxygen atoms in the polyoxoanion building block in terms of the coordinated method of the oxygen atoms: terminal oxygen Ot, terminal oxygen Ot′ linked to La^{3+}, double-bridging oxygen Ob, and central oxygen Oc. Thus, the

dx.doi.org/10.1021/cg500955d | *Cryst. Growth Des.* 2015, 15, 103−114

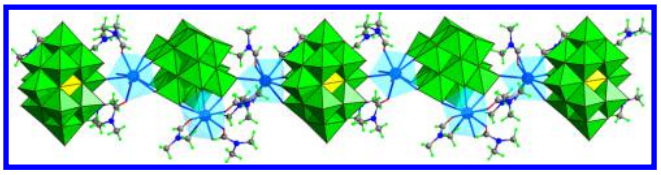

Figure 1. Polyhedral and ball-and-stick representation of 1D chain in compound **1**. Color codes: Mn (yellow), V (green), La (blue), C (gray), N (dark blue).

V−O distances can be divided into four groups: V−Ot 1.585−1.617 Å, V−Ot′ 1.620−1.661 Å, V−Ob 1.697−2.018 Å, and V−Oc 1.859−2.415 Å in **1**. The central Mn−O bond lengths are 1.877−1.924 Å, and the O−Mn−O angles are in the range of 87.3(1)−177.2(2)°. The bond lengths and angles of $\{MnV_{13}\}$ polyoxoanion are in agreement with those in the reported literature.[10]

As shown in Figure 2, there are two crystallographically independent La^{3+} cations in the structure, and each La^{3+} cation

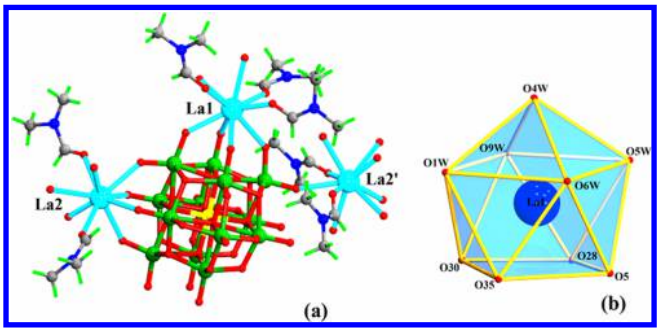

Figure 2. (a) Ball-and-stick representation of the $[\{La_2(DMF)_5(H_2O)_4\}\{MnV_{13}O_{38}\}]^-$ unit in **1**; (b) the coordination environments of the La^{III} cation.

adopts a nine-coordinate tricapped trigonal prismic geometry, with La−O distances of 2.455−2.653 Å. The La(1) ion is defined by four terminal oxygen atoms from the $\{MnV_{13}\}$ polyoxoanions (La−O_{POM} 2.536−2.654 Å), three oxygen atoms from the DMF ligands (La−O 2.498−2.537 Å), and two coordination oxygen atoms from solvent water molecules (La−O_{aqua} 2.555 and 2.592 Å). The La(2) ion is coordinated by two aqua ligands (La−O_{aqua} 2.555 and 2.592 Å), two oxygen atoms from two DMF ligands (La−O 2.498−2.537 Å), and five terminal oxygen atoms from two $\{MnV_{13}\}$ anions (La−O_{POM} 2.536−2.654 Å). Five independent DMF molecules act as monodentate ligand and link to two La cations. As far as $\{MnV_{13}\}$ polyoxoanion, it coordinates to three La atoms through nine terminal oxygen atoms. As shown in Figure 1, each $\{MnV_{13}\}$ with tridentate ligand mode coordinates to two $[La(2)(DMF)_2(H_2O)_2]^{3+}$ (as linker) and one $[La(1)(DMF)_3(H_2O)_2]^{3+}$ (as capping unit) subunits via the terminal oxygen atoms to construct a one-dimensional chain-like structure. As shown in Figure 3, neighboring chains are further connected through C−H···O hydrogen bonding interactions into two-dimensional (2D) layers (C−H···O = 1.75 Å) in the structure. However, the adjacent sheets form staggered arrangement and stack in an ABAB··· sequence but not well-overlapped to each other (Figure 4). The distance between the layers is approximately 9.119 Å, and free water and DMF molecules locate in the interlayers. The abundant intermolecular hydrogen-bonding weaker force is very important in the stability of a three-dimensional (3D) supramolecular framework. To our

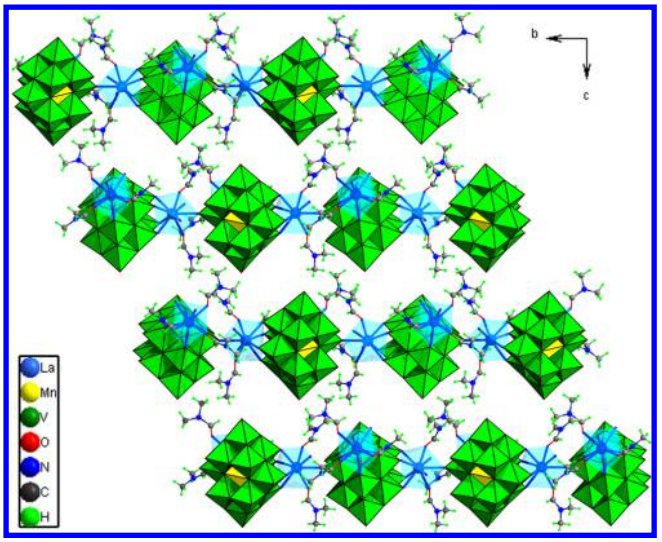

Figure 3. Polyhedral and ball-and-stick representation of 2D supramolecular layer in **1**.

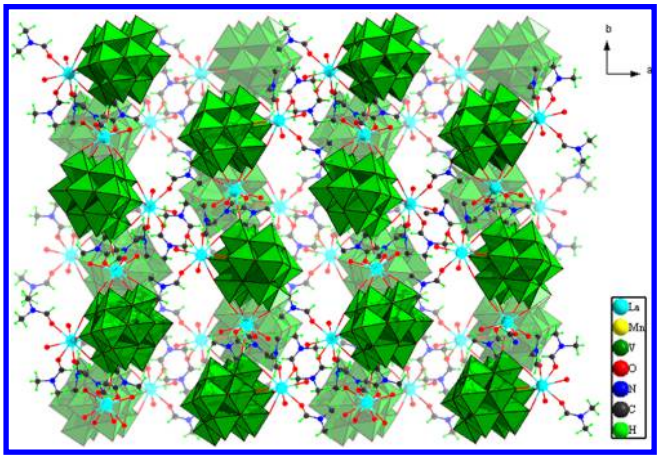

Figure 4. 3D alternately supramolecular assembly of compound **1** along the *c* axis.

best knowledge, compound **1** represents the first example of inorganic−organic hybrid constructed of $\{MnV_{13}\}$ polyoxoanions based on lanthanide-organic coordination units covalently connecting.

Crystal Structure of ***2***. Compound **2** possesses a similar one-dimensional chain structure with **1**. The structural asymmetric unit of **2** is composed of two $\{MnV_{13}\}$ polyoxovanadate anions, four crystallographically unique Ce cations, four DMF ligands, DMF solvent, and lattice water molecules. As seen in Figure 6a, all the Ce cations adopt a nine-coordinate geometry with tricapped trigonal prismic construction, whereas the coordination environments of Ce(1), Ce(2), Ce(3), and Ce(4) are different. The Ce(1) cation is coordinated by four solvent water molecules, four oxygen atoms from one $\{MnV_{13}\}$ anion (Ce−O_{POM} 2.455−2.653 Å), and one oxygen atom from the DMF ligand (Ce−O 2.498−2.537 Å); the coordination geometry of Ce(2) ion is defined by three solvent water molecules (Ce−O_{aqua} 2.555−2.592 Å), five terminal oxygen atoms from two $\{MnV_{13}\}$ anions (Ce−O_{POM} 2.455−2.653 Å), and one oxygen atom from the DMF ligand (Ce−O 2.498−2.537 Å). Ce(3) and Ce(2) cations possess a similar coordination environment, as well as Ce(4) and Ce(1) cations have the same coordination environment. The average Ce−O bond length is 2.464 Å.

dx.doi.org/10.1021/cg500955d | *Cryst. Growth Des.* 2015, 15, 103−114

There are four crystallographic independent DMF ligands which act as monodentate ligand and adopt the same connection mode corresponding to that in compound **1**. As shown in Figure 5, the structure of **2** exhibits a chain assembled by $[MnV_{13}O_{38}]^{7-}$ polyoxoanions and $[Ce(DMF)(H_2O)_3]^{3-}$ as linkers.

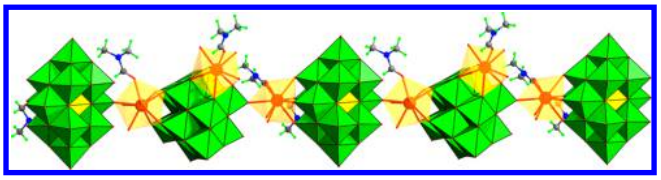

Figure 5. Polyhedral and ball-and-stick representation of the 1D chain in compound **2**.

The Ce-DMF complex connected the $[MnV_{13}O_{38}]^{7-}$ polyoxoanion into a one-dimensional chain, and adjadcent chains are linked to form a 2D supramolecular sheet through hydrogen-bonding interactions. And then these layers based on $\{MnV_{13}\}$ aions and Ce-DMF moieties are further connected to a 3D supramolecular structure. According to this coordination mode, the 3D structure generates an interesting supramolecular channel along the *a* axis, dissociated DMF and lattice water molecules locate in the channels. It is notable that the adjacent supramolecular layers in compound **2** are well-overlapped and form an AAAA··· arrangement mode (Figure 7).

Crystal Structure of **3**. Single-crystal X-ray diffraction analysis of compound **3** reveals that the basic unit is constructed of $[MnV_{13}O_{38}]^{7-}$ building blocks, DMF molecule, and Nd^{3+} and K^+ cations. In compound **3**, the structure of $[MnV_{13}O_{38}]^{7-}$ is similar to the central polyoxoanion in compound **1**. The bond lengths of V−O range from 1.581 to 2.458 Å. The central Mn−O bond lengths are in the range of 1.849−1.920 Å, and the O−Mn−O angles are 86.2(2)−178.4(2)°. As seen in Figure 8, there is one crystallization-independent Nd atom in **3**, which adopts nine-coordinated

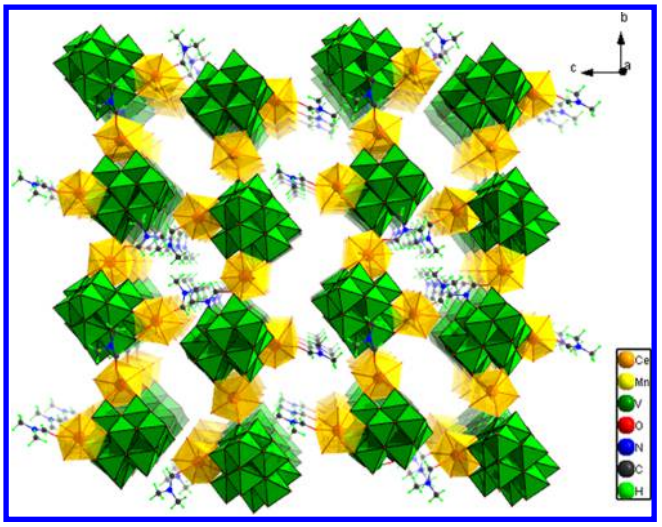

Figure 7. Polyhedral and ball-and-stick representation of the 3D supramolecular framework in compound **2**.

geometry defined by five terminal oxygen atoms from two polyoxoanions (Nd−O_{POM} = 2.409−2.610 Å), one oxygen atom from DMF molecule (Nd−O = 2.386 Å), and three aqua ligands (Nd−O_{aqua} = 2.479−2.525 Å). The average Nd−O bond length is 2.500 Å. In addition, there are two crystallographically unique potassium ions distributed around the $[\{Nd(DMF)(H_2O)_3\}\{MnV_{13}O_{38}\}]^{4-}$ cluster, which are coordinated by two $\{MnV_{13}\}$ polyoxoanions through five terminal oxygen atoms (K−O 2.706−3.017 Å) and three water molecules (K−OH_2 2.704−3.003 Å).

It is notable that the involvement of countercations promotes the construction of a unique architecture with 3D open framework in compound **3**. Each DMF molecule as a monodentate ligand connects the Nd^{3+} cation to form an Nd-DMF complex unit. The $[Nd(DMF)(H_2O)_3]^{3+}$ subunits link $\{MnV_{13}\}$ building blocks alternately to form a one-

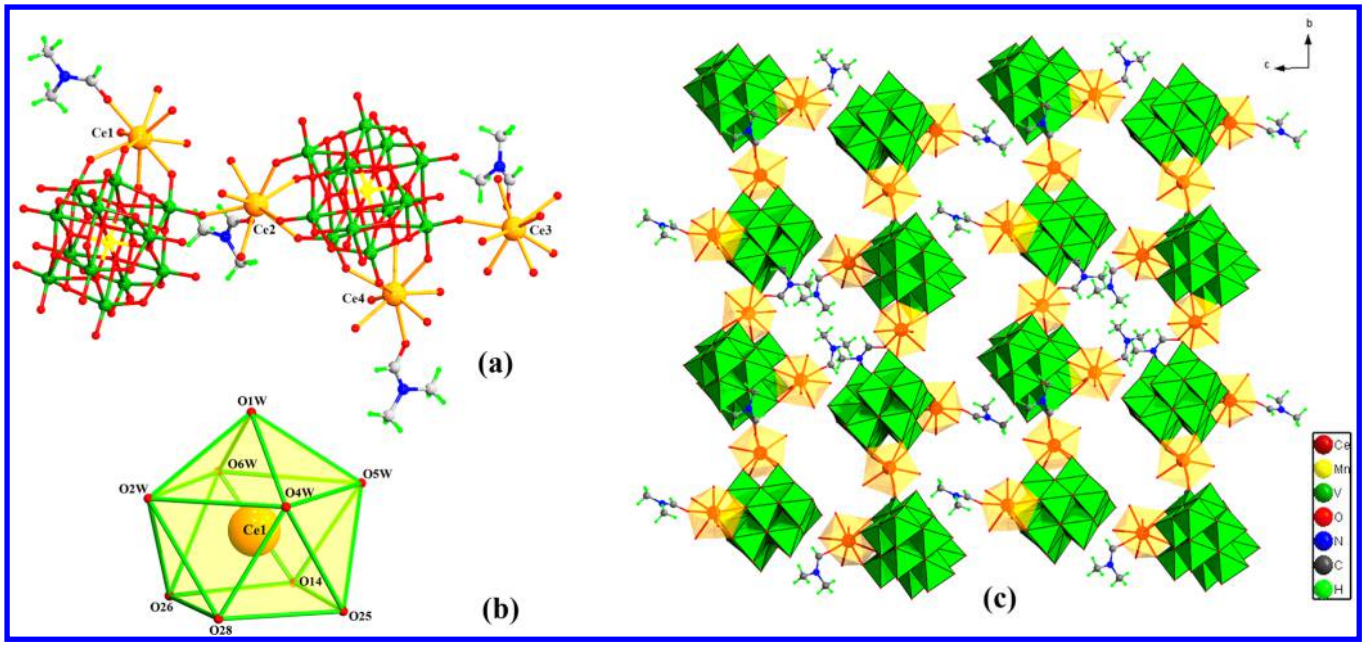

Figure 6. (a) Ball-and-stick representation of the $[\{Ce_2(DMF)_2(H_2O)_7\}\{MnV_{13}O_{38}\}]^-$ unit in **2**; (b) the coordination environments of the Ce^{III} cation; (c) view of the crystal packing of compound **2** along the *a* axis.

dx.doi.org/10.1021/cg500955d | *Cryst. Growth Des.* 2015, 15, 103−114

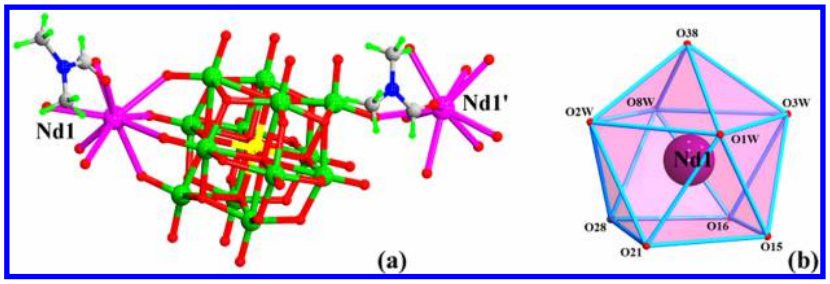

Figure 8. (a) Ball-and-stick representation of the $[\{Nd(DMF)(H_2O)_3\}\{MnV_{13}O_{38}\}]^{4-}$ unit in **3**; (b) the coordination environments of the Nd^{III} cation.

dimensional chain (Figure 9). The neighboring chains are connected by K^+ cations to construct 2D layers (Figure 10).

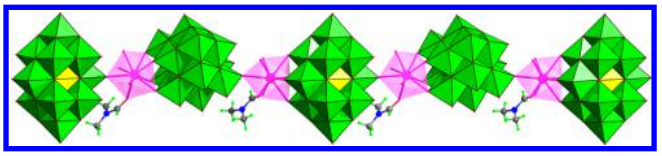

Figure 9. Polyhedral and ball-and-stick representation of a 1D chain in compound **3**.

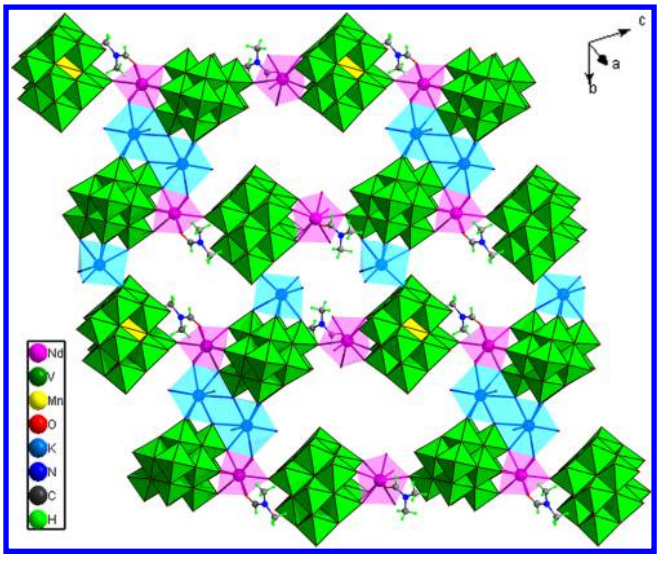

Figure 10. Polyhedral view of the 2D network in compound **3**.

Furthermore, potassium cations link these 2D layers and lead to the formation of a 3D network structure with channels along the *a* axis. The 16-ring window-type channel is built from 12 V, two Nd and two K atoms, and the section size of the channel is approximately 11.9 × 5.5 Å. Free solvent water molecules locate in the tunnels (Figure 11).

Recently, it has been discovered that single molecules of POMs self-assemble to form large entities with soft-matter properties; these soft-state oxometalates have been proposed to be called soft-oxometalates (SOMs).[14] Compounds **2** and **3** might be the potential precursors to the formation of soft-oxometalates in dispersion based on the supramolecular structures.

Crystal Structure of 4 and 5. Single-crystal X-ray diffraction analyses reveal that compounds **4** and **5** are isostructural, and the unit cell dimensions, volumes, related bond distances and angles are only slightly different. Therefore, only the structure

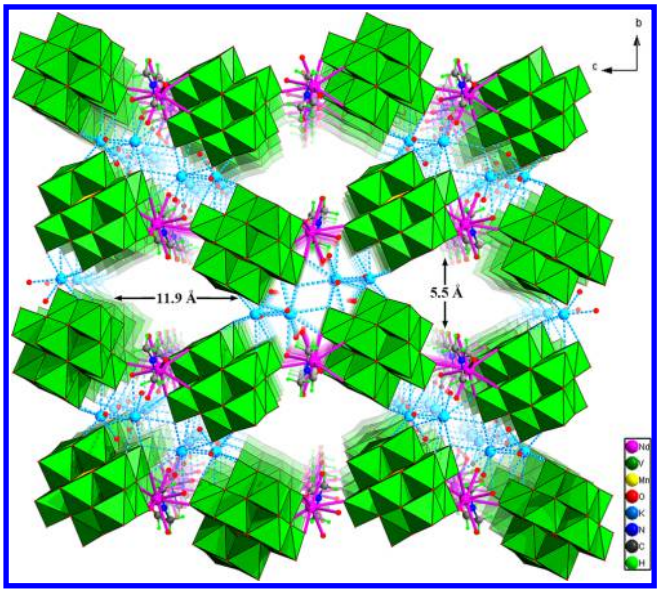

Figure 11. Polyhedral and ball-and-stick representation of the $[MnV_{13}O_{38}]^{7-}$ polyoxoanions connected by Nd^{3+} and K^+ into a 3D framework with channels in compound **3**.

of compound **4** is described in detail. Compound **4** shows a 3D supramolecular open framework, and the basic structural unit of **4** is composed of $[MnV_{13}O_{38}]^{7-}$ building blocks, Ln-isonicotinic acid coordination subunits, and lattice water molecules. The $[MnV_{13}O_{38}]^{7-}$ cluster is composed of a central $\{MnO_6\}$ octahedra surrounded by 13 edge-shared $\{VO_6\}$ octahedra. There are four kinds of oxygen atoms in the polyoxoanion building block in terms of the method of oxygen atoms that are coordinated and the V−O distances can be divided into four groups: V−Ot 1.576−1.616 Å, V−Ot′ 1.621−1.664 Å, V−Ob 1.698−2.388 Å, and V−Oc 2.061−2.361 Å in **4**. The central Mn−O bond lengths are 1.855−1.923 Å, and the O−Mn−O angles are in the range of 87.1(2)−178.6(2)°. As shown in Figure 12, two crystallographically unique La ions in the complex, La(1) and La(2), adopt a nine-coordinate polyhedron with tricapped trigonal prismic coordination geometry, whereas their coordination environments are different. The La(1) cation links five terminal oxygen from two $\{MnV_{13}\}$ clusters (La−O_{POM} 2.536−2.654 Å), one carboxyl oxygen from one isonicotinic acid (La−$O_{carboxyl}$ 2.498−2.537 Å), and three water molecules (La−O_{aqua} 2.555 and 2.592 Å). La(2) cation is linked by four terminal oxygen atoms from one $\{MnV_{13}\}$ anion (La−O_{POM} 2.536−2.654 Å), two carboxyl oxygen atoms from two isonicotinic acid ligands (La−$O_{carboxyl}$ 2.498−2.537 Å) and two aqua ligands (La−O_{aqua} 2.555 and 2.592 Å).

dx.doi.org/10.1021/cg500955d | *Cryst. Growth Des.* 2015, 15, 103−114

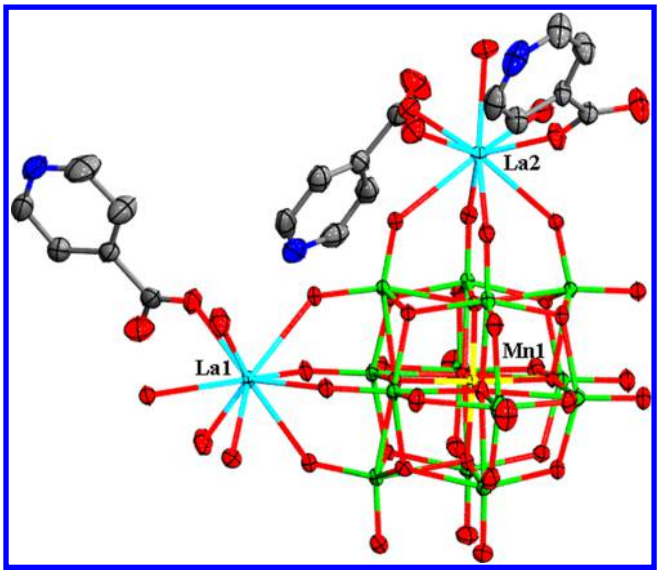

Figure 12. ORTEP drawing of **4** with thermal ellipsoids at 50% probability.

In compound **4**, $[MnV_{13}O_{38}]^{7-}$ polyoxoanions and La (1)-isonicotinic acid coordination complexes are connected alternately to form a one-dimensional chain. La (2) atom caps on the other side of the $\{MnV_{13}\}$ building block through four terminal oxygen atoms, and all the rare-earth cations form a wavelike arrangement (Figure 13). Furthermore, the adjacent

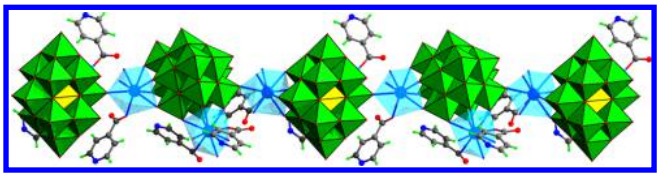

Figure 13. Polyhedral and ball-and-stick representation of the 1D chain in compound **4**.

chains are interconnected to form a 2D supramolecular layer through a weaker hydrogen-bonding force (Figure 14). The structure of isonicotinic acid ligands is in agreement with that described in the literature[15] (C−C 1.356−1.529 Å; C−N 1.320−1.341 Å). The packing of layers in compound **4** generates supramolecular channels along the *b* axis, which are filled by lattice aqueous molecules and isonicotinic acid ligands. Extensive hydrogen-bonding interactions exist among the free water molecules, polyoxoanions, isonicotinic acid molecules, and water molecules coordinated to the La^{3+} and play an important role in the stability of the 3D supramolecular structure. The bond valence sum calculations indicated that the Mn site is in the +4 oxidation state, all V sites are in the +5 oxidation state, and all La sites are +3 oxidation states.

Crystal Structure of ***6***. The basic structural unit of **6** constitutes two $\{MnV_{13}\}$ anions, three crystallographically independent Pr cations, two isonicotinic acid ligands, and lattice water molecules. The structure of $[MnV_{13}O_{38}]^{7-}$ precursor is maintained in **6**. As revealed by X-ray crystallographic analysis, the bond lengths of V−O are in the range of 1.571−2.429 Å. The bond lengths of central Mn−O range from 1.849 to 1.913 Å, and the O−Mn−O angles range from 87.1 (2) to 176.2 (2)°. As seen in Figure 15, three crystallographically unique Pr (III) cations exist in the asymmetric unit.

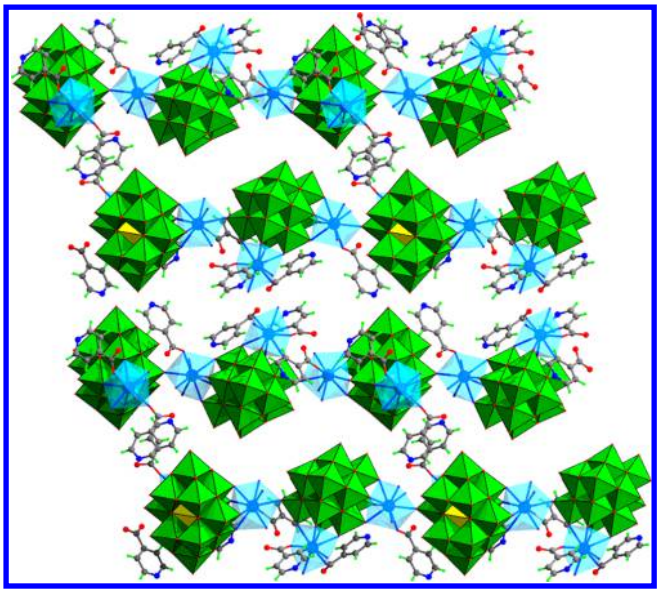

Figure 14. Polyhedral and ball-and-stick representation of the 2D supramolecular layer in compound **4**.

Pr (1) and Pr (2) join neighboring $[MnV_{13}O_{38}]^{7-}$ cluster alternately as linker, while Pr (3) caps on the other side of polyoxoanions. Pr(1) is connected by five oxygen atoms from two $[MnV_{13}O_{38}]^{7-}$ units (Pr−O 2.496−2.646 Å), one carboxyl oxygen from one isonicotinic acid ligand (Pr−O 2.376 Å), and three water molecules (Pr−OH_2 2.479−2.553 Å), adopting a disorted tricapped trigonal prism coordination environment. Pr (2) links to five oxygen atoms from two $[MnV_{13}O_{38}]^{7-}$ anions (Pr−O 2.445−2.605 Å) and four water molecules (Pr−OH_2 2.486−2.522 Å). Pr (3) ion is coordinated by four terminal oxygen atoms from one $\{MnV_{13}\}$ polyoxoanion (Pr−O 2.535−2.678 Å), one carboxyl oxygen atom from isonicotinic acid molecule (Pr−O 2.480 Å) and four water molecules (Pr−OH_2 2.489−2.546 Å). The average bond length of Pr−O is 2.528 Å in **6**. There are two kinds of crystallographically independent isonicotinic acid molecules in the structural unit, which coordinates to Pr (III) cations via carboxyl oxygen atom as a monodentate mode.

In the structure, Pr (1) and Pr (2) as tether link to $\{MnV_{13}\}$ polyoxoanions by a corner-sharing fashion alternately to construct an extended 1D chain (Figure 16). The neighboring organic−inorganic chains based on $\{MnV_{13}\}$ are further connected into a 3D supramolecular framework through weaker hydrogen-bonding interactions. It is interesting that the stacking mode forms ca. 7.56 × 13.21 Å channels along the *a* axis (Figure 17). Likewise, free isonicotinic acid and lattice water molecules reside in the channels and are involved in the hydrogen-bonding interactions to stabilize the framework.

Discussion of Structure Evolution. Single-crystal X-ray diffraction analyses revealed that complexes **1**−**3** crystallized in the space group P_{bca}, $P\bar{1}$, and $P2_1/n$, respectively. Although compounds **1**−**3** were prepared using a similar procedure, it is interesting to observe that they show three different structures on going from La to Nd, which provides profound insights into the critical influence of lanthanide contraction. The effect of lanthanide contraction on the formation of structures has been extensively reported for lanthanide coordination polymers, in which as the ionic radii of the lanthanide ions decreases with increasing atomic number, and the increasingly important ligand−ligand repulsion leads to the variations of coordination

dx.doi.org/10.1021/cg500955d | *Cryst. Growth Des.* 2015, 15, 103−114

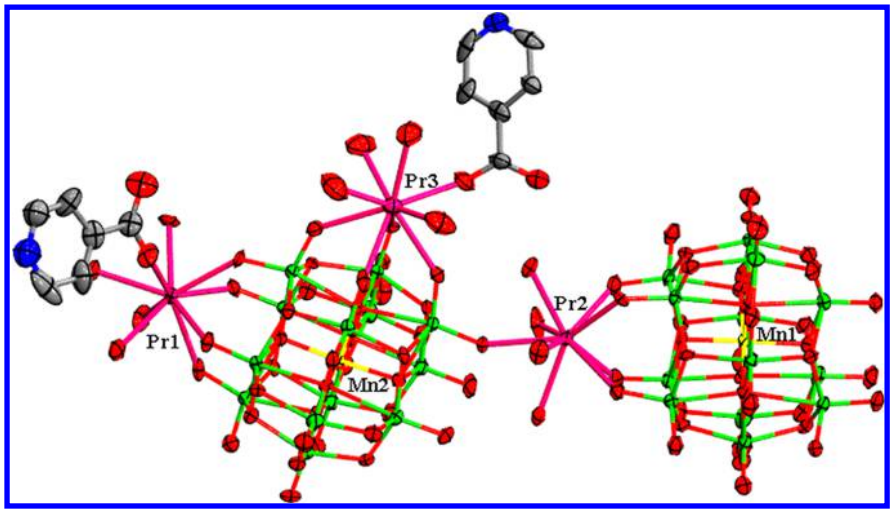

Figure 15. ORTEP drawing of **6** with thermal ellipsoids at 50% probability.

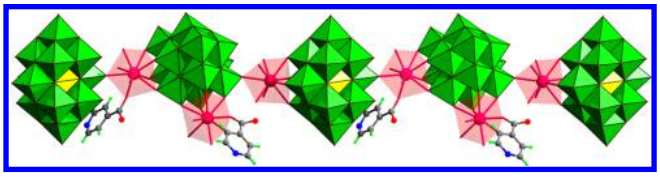

Figure 16. Polyhedral and ball-and-stick representation of the 1D chain in compound **6**.

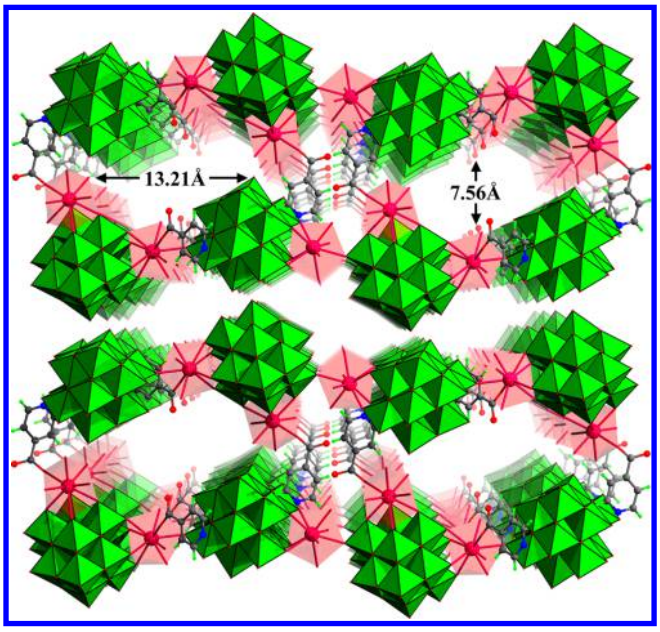

Figure 17. Polyhedral and ball-and-stick representation of the 3D supramolecular framework with channels in compound **6**.

number and ligand coordination modes around each metal ion.[16] Recently, the effect of lanthanide contraction on structures have also been observed in POM-lanthanide complexes. In 2010, An et al. reported a series of POM-lanthanide complexes based on $[BW_{11}O_{39}H]^{8-}$ polyanion, the structures of which varied from 3D frameworks into 0D clusters when the lanthanide cations changed from Ce^{3+} and Nd^{3+} to Eu^{3+} and Sm^{3+}.[17a] Zhang's group prepared several POM-lanthanide complexes based on Preyssler anions, the structural variation of which from 2D frameworks to supporting clusters is attributed to the lanthanide contraction effect.[17b] However, compared to the extensively studies on the lanthanide contraction effect in the formation of lanthanide coordination polymers, studies on the lanthanide contraction effect in the formation of POM-lanthanide complexes are still limited.

As seen in Figure 18, the organic constituents in the compounds **1**−**3** gradually reduce when rare earth ions

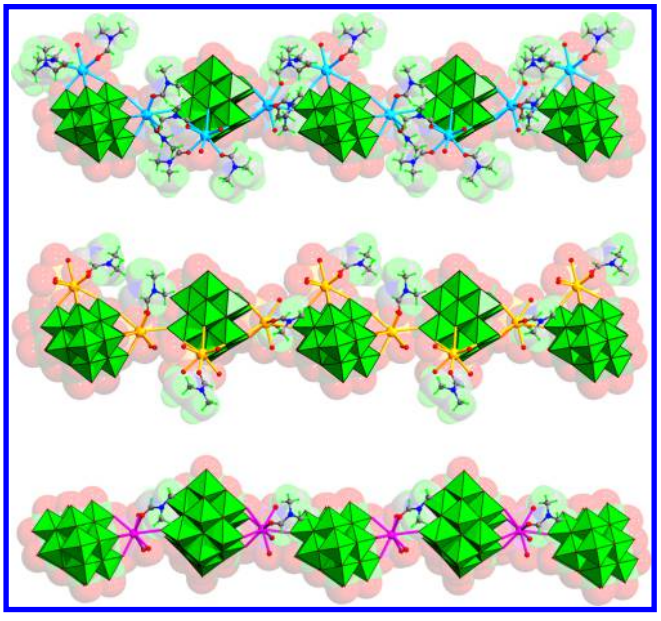

Figure 18. Comparison of 1D chains in compounds **1**−**3**.

modulate from La, Ce, to Nd, and the proportion of DMF to $[MnV_{13}O_{38}]^{7-}$ polyoxoanion are 5:1, 2:1, and 1:1, respectively. This phenomenon is probably caused by the lanthanide contraction effect. The contraction of the metal radius is reflected in the decrease of the bonding Ln−O distances with increasing atomic number in compounds **1**−**3**. Variation of the mean lanthanide−oxygen bond lengths with the atomic number for compounds **1**−**3** is as shown in Figure 19 ($Ln-O_{POM} > Ln-O_{aqua} > Ln-O_{ligand}$), although differences among the three types of bonds are subtle. The Ln−O bond lengths tend to linearly decrease as the lanthanide atomic number increases owing to the well-known contraction effect in rare-earth metals,

dx.doi.org/10.1021/cg500955d | *Cryst. Growth Des.* 2015, 15, 103−114

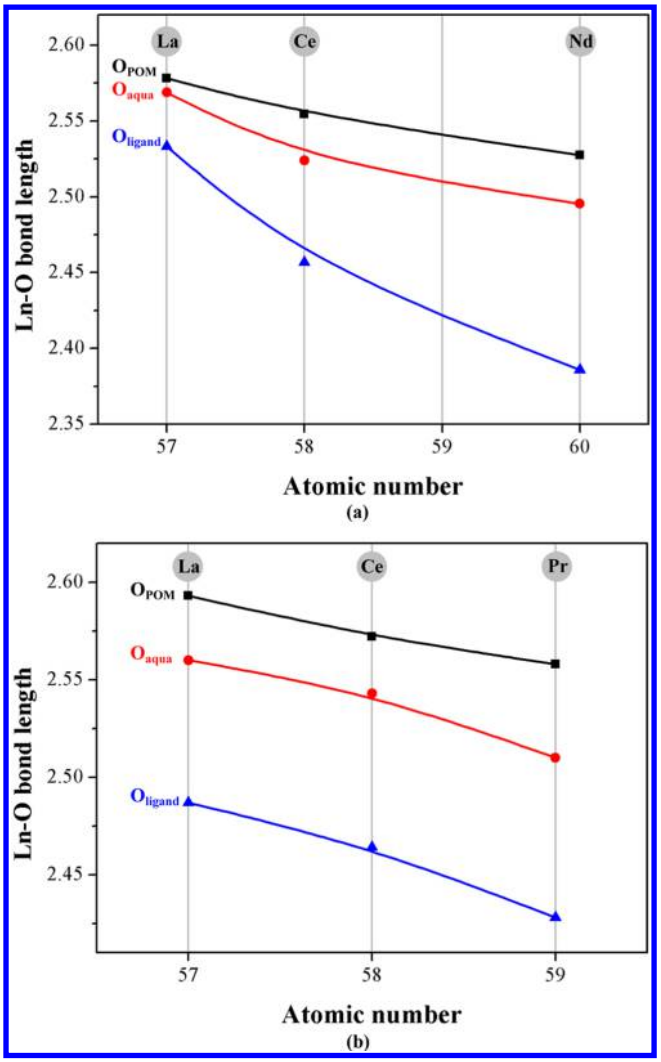

Figure 19. Variation of the mean lanthanide−oxygen bond lengths with the atomic number for compounds **1**−**3** (a) and **4**−**6** (b). Abbreviations: O_{POM}, O atoms bridging POM clusters between lanthanides; O_{aqua}, O atom from a terminal aqua water molecule; O_{ligand}, O atom from a terminal organic group.

but variations in this series do not exceed 0.15 Å. It is worth mentioning that, while those bonds that involve O atoms of compounds **1**−**3** show parallel decreasing trends when going from La to Nd, the Ln−O_{ligand} bonds undergo more pronounced shortening, and the Ln−O_{POM} bonds remain nearly constant through the series. With the interaction force between rare earth cations and polyoxoanions gradually enhanced, available space among the anions decreases, so the coordination number of DMF molecules decreases. Compound **1** contains the most number of DMF molecules,and the distances between the adjacent chains are far due to the space steric hindrance. In order to achieve the most close packing mode to reduce the energy of the system, the adjacent supramolecular 2D sheets staggered in an ABAB··· fashion to form 3D supramolecular structure in compound **1**, whereas the 2D supramolecular layers appear in a parallel arrangement in compound **2**, forming supramolecular channels along the *a* axis. Because of containing the least number of DMF, the steric-hindrance effect is weak in compound **3**. The POM-rare earth chains are further connected by potassium cations to construct a 3D open framework structure.

Table 2. Comparison of Ln−O Bond Lengths in 1−3

compounds	range of Ln−O lengths (Å)	average Ln−O lengths (Å)
1 (La^{III})	2.455−2.654	2.561
2 (Ce^{III})	2.386−2.648	2.536
3 (Nd^{III})	2.386−2.610	2.501

The influence of the lanthanide contraction effect on structures is also reflected in the structural changes of compounds **4**−**6**. For compounds **4**−**6**, the organic constituents gradually reduce when rare earth ions modulate from La, Ce, to Pr, and the ratio of isonicotinic acid to $[MnV_{13}O_{38}]^{7-}$ polyoxoanion changes from 3:2 to 2:1. Compounds **4** and **5** are isostructural, which exhibit a 1D chain structure. Compound **6** reveals a 3D supramolecular structure with a type of channel of approximately 7.56 × 13.21 Å. Likewise, the bonding lengths of Ln−O increased based on the contraction of rare earth radius in compounds **4**−**6** (La−O average values 2.565 Å for **4**, Ce−O average value 2.544 Å for **5**, Pr−O average value 2.528 Å for **6**).

Electrochemical Analyses and Electrocatalytic Activities. The electrochemical behaviors of compounds **1**−**6** and their electrocatalytic properties for nitrate were studied. The cyclic voltammetric behavior for **1** in pH 4 (0.4 M CH_3COONa-CH_3COOH) buffer solution exhibits three pairs of redox peaks in the potential range of +1.4 to −0.8 V, and the mean peak potentials $E_{1/2} = (E_{pa} + E_{pc})/2$ are 0.804 V, 0.203 V, and −0.37 V (vs Ag/AgCl), respectively (Figure S4a). The first oxidation peak I (+0.912 V) and its reduction counterpart I′ (+0.696 V) are attributed to the redox process of the Mn centers.[18] The second and third oxidation peaks II and III (+0.297 V and −0.126 V, respectively) and their reduction counterparts II′ and III′ (+0.109 V and −0.614 V) are all ascribed to the vanadium-centered reductions, ($V^V \rightarrow V^{IV}$) and ($V^{IV} \rightarrow V^{III}$), respectively.[19] The electrochemical properties of compound **2** were also detected in the pH 4 (0.4 M CH_3COONa + CH_3COOH) buffer solution (Figure 20). There are three reduction peaks that appear in the potential range of +1.4 to −0.8 V, with peak potentials located respectively at 0.809 V, 0.226 V and −0.375 V versus the Ag/AgCl electrode. The oxidation peak located at 0.923 V and its reduction counterpart located at 0.695 V correspond to the redox processes of the Mn^{IV}, similar to that of **1**. The last two peaks at 0.226 V and −0.375 V are assigned to the redox process of V^V centers. The electrochemical properties of compound **3** were also detected in the pH 4 media, which is similar to **1**. As shown in Figure S5a, there are three redox couples located at the positive domain and the mean peak potentials $E_{1/2} = (E_{pa} + E_{pc})/2$ are 0.831 V, 0.219 V, and −0.389 V (vs Ag/AgCl), which are ascribed to the Mn and V centers.

We have also investigated the electrochemical behaviors of compounds **4**−**6** in pH 4 (0.4 M CH_3COONa + CH_3COOH) buffer solution at different scan rates. As shown in Figure S6a, the cyclic voltammogram of compound **4** reveals three pairs of redox peaks in the potential range from +1.4 V to −0.8 V. The first oxidation peak I (+0.882 V) and its corresponding counterpart reduction peak I′ (+0.607 V) are attributed to the manganese centers reductions. The second and third oxidation peaks II and III (+0.423 V and −0.118 V) and their reduction counterparts II′ and III′ (+0.112 V and −0.0.072 V) are attributed to redox process of the V centered ($V^V \rightarrow V^{IV}$) and ($V^{IV} \rightarrow V^{III}$). The mean peak of potentials $E_{1/2} = (E_{pa} + E_{pc})/2$ are 0.745 V, 0.268 V, and −0.095 V (vs Ag/AgCl), respectively.

dx.doi.org/10.1021/cg500955d | *Cryst. Growth Des.* 2015, 15, 103−114

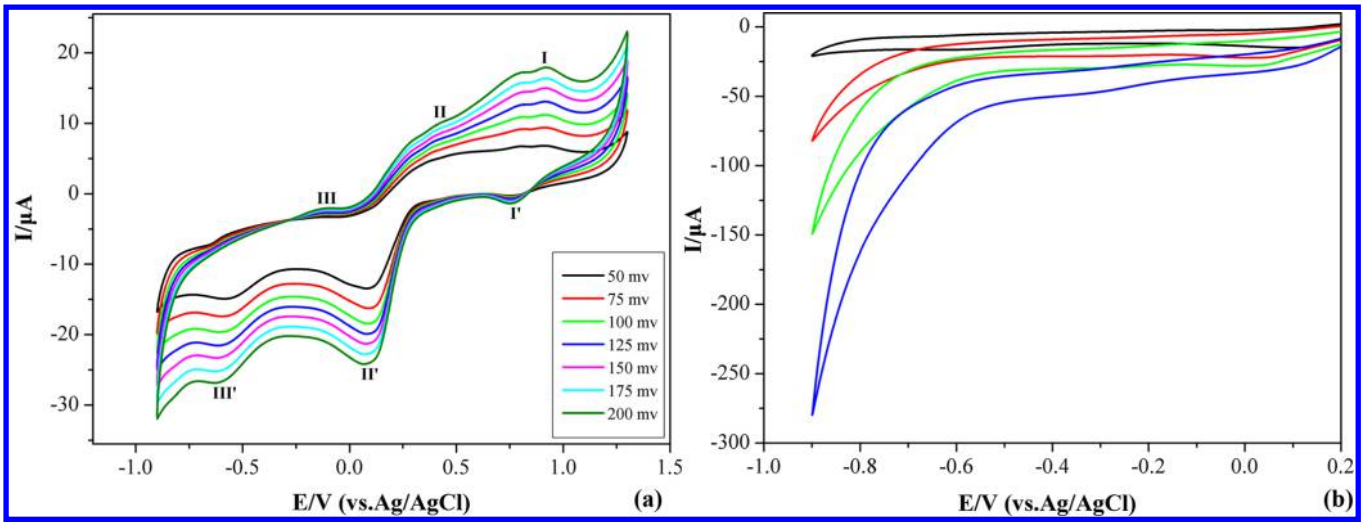

Figure 20. (a) Cyclic voltammograms of 2×10^{-4} M **2** in the pH = 4.0 (0.4 M CH_3COONa + CH_3COOH) buffer solution at different scan rates (from inner to outer: 25, 50, 75, 100, 125, 150, 175, 200 mV s^{-1}); (b) Electrocatalysis of the reduction of NO_2^- in the presence of 2×10^{-4} M **2** at the scan rate of 150 mV s^{-1}. The concentrations of NO_2^- are (i) 0.0, (ii) 1.0, (iii) 2.0, and (iv) 4.0 mM. The working electrode was glassy carbon, and the reference electrode was Ag/AgCl.

As seen in Figure S7a, there are three redox peaks appear in compound **5** in the potential range +1.4 to −0.8 V, and the mean peak potentials are 0.813 V (I−I′) and 0.197 V (II−II′) and −0.368 V (III−III′) (vs Ag/AgCl), respectively. The three peaks correspond to the redox of the Mn and V in the polyoxoanion framework. The electrochemical properties of compound **6** were also detected in the pH 4 media, which is similar to **5**. As shown in Figure S8a, there are three redox couples located at the positive domain, and the mean peak potentials $E_{1/2} = (E_{pa} + E_{pc})/2$ are 0.779 V, 0.240 V, and −0.108 V (vs Ag/AgCl), which are ascribed to the Mn and V centers. Further, the CV of **1**−**6** at different scan rates showed that the peak currents of the redox process were proportional to the scan rate, indicating that the redox process on the glassy carbon (GC) electrode is surface-controlled (Figure S9, Supporting Information).

The determination and elimination of nitrite ions in environmental and food samples have been paid considerable attention in recent years due to their distinct toxicity and suspected carcinogenicity.[20] Generally, it is difficult to directly electroreduce the nitrite ions to their corresponding reduced form with the bare electrode because this process requires high overpotential at most of the bare electrode surfaces. However, the introduction of various catalysts into the bare electrodes could speed up the electroreduction process and lower the overpotential. In this aspect, POMs are one kind of suitable catalyst candidate because POMs are capable of delivering electrons to other species, serving as powerful electron reservoirs for multielectron reductions.[21]

On the basis of the aforementioned background, the electrocatalytic reduction properties of the {MnV_{13}}-based organic−inorganic hybrids **1**−**6** were further investigated toward the reduction of nitrite in the same buffer solution as those employed in the CV studies. Figure S4b shows the CV of the electrocatalytic reduction of nitrite for **1** detected in the pH 4 (0.4 M CH_3COONa + CH_3COOH) buffer solution. With the addition of modest amounts of nitrite, the reduction peak currents at the potential domain of V increased, while the corresponding oxidation peak currents dramatically decreased, suggesting that nitrite was reduced by the reduced POM species. It deserves to be mentioned that the catalytic activity is enhanced when the extent of the polyoxoanion reduction is increased. For **2** and **3**, the CV for the electrocatalytic reduction of nitrite was also observed under similar conditions, and compound **3** exhibits the best catalytic effect of nitrite. It can be clearly seen the reduction peak currents of the vanadium at the potential domain also enhance sharply, indicating that compounds **2** (Figure 20b) and **3** (Figure S5b) exhibit electrocatalytic activity for nitrite reduction.

Figure S6b illustrates the ability of compound **4** to electrocatalyze the reduction of nitrite. In the explored potential domain, the onset of the catalytic process is at about 0.2 V and is triggered by the wave of the vanadium. Upon increasing nitrite concentration, the cathodic current of the reduction wave rises, and the corresponding anodic current gradually decreases. The catalytic effect for electrocatalytic nitrite is still observed in compounds **5** and **6**. (Figures S7b and S8b). The results indicated that **1**−**6** display excellent electrocatalytic activity toward the reduction of nitrite. In comparison, no reduction of nitrite took place on the GC electrode in the absence of compounds. Other challenging electrocatalytic processes such as reduction of bromate, chlorate, iodate, and hydrogen peroxide will be explored. In addition, it is expected that new {MnV_{13}}-based organic−inorganic hybrids with appropriate compositions will expand application domains.

Magnetic Properties. The variable temperature magnetic susceptibility of compound **2** was investigated in the temperature range of 2.0−300 K at a 0.1 T magnetic field on the single crystalline samples. The value of χ_m increases gradually from 0.011 cm^3 mol^{-1} at 300 K to 0.054 cm^3 mol^{-1} at 50 K, exponentially to the maximum of 0.677 cm^3 mol^{-1} at 2 K. The $\chi_m T$ vs T plot decreases continuously with decreasing temperature, revealing the characteristic of antiferromagnetic interactions. At room temperature, the experimental $\chi_m T$ value (3.472 cm^3 K mol^{-1}) of **2** is approximately equal to the theoretical value (3.481 cm^3 K mol^{-1}) for two Ce^{III} ions (1.606 cm^3 K mol^{-1}, $^2F_{5/2}$, $J = 5/2$, $g_J = 6/7$) and one isolated spin-only Mn^{IV} (1.875 cm^3 K mol^{-1}, $S = 3/2$, $g = 2.0$). As shown in Figure 21, the magnetic susceptibility of **2** follows the Curie−

dx.doi.org/10.1021/cg500955d | Cryst. Growth Des. 2015, 15, 103−114

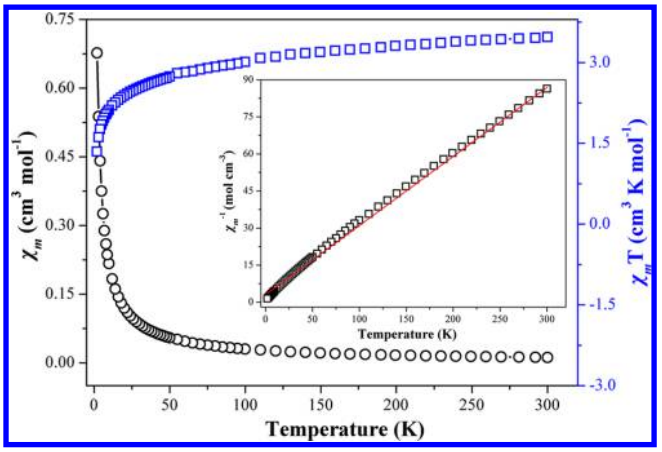

Figure 21. Temperature dependence of χ_m (○), $\chi_m T$ (□) values and (inset) temperature dependence of reciprocal magnetic susceptibility χ_m^{-1} for **2**. The red line is the best fit with the Curie–Weiss law.

Weiss law, $\chi_m = C/(T - \theta)$ with a Curie constant C = 3.520 cm^3 K mol^{-1} and a Weiss constant θ = −11.246 K in the temperature range of 2–300 K. These Curie constants are in reasonably good agreement with the expected value. The negative Weiss temperatures suggest the presence of antiferromagnetic interactions in compound **2**. For **5**, the $\chi_m T$ value slowly decreases from 3.452 cm^3 K mol^{-1} at 300 K to 1.923 cm^3 K mol^{-1} at 2 K, revealing antiferromagnetic interaction in **5** (Figure 22). The χ_m^{-1} vs T curve is fitted with the Curie–Weiss

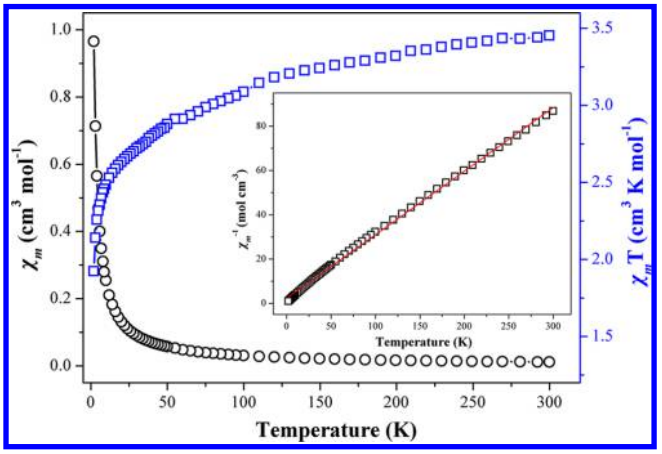

Figure 22. Temperature dependence of χ_m (○), $\chi_m T$ (□) values and (inset) temperature dependence of reciprocal magnetic susceptibility χ_m^{-1} for **5**. The red line is the best fit with the Curie–Weiss law.

law, leading to a Curie constant of 3.486 cm^3 K mol^{-1}. The Weiss temperature (θ) of −8.138 K indicates a weak antiferromagnetic interaction in **5**. Magnetic studies indicate that antiferromagnetic interactions exist in compounds **3** and **6** (Figures S10 and S11).

FT-IR and UV–vis Spectroscopy. There are a broad band at 3422 cm^{-1} and a strong peak at 1645 cm^{-1} in the IR spectrum of compound **1**, which are assigned to the lattice and coordinated water molecules (Figure S12). The characteristic peaks at 977, 924, 829, 652, 594 cm^{-1} are attributed to ν (V═O) and ν (V–O–V) of the $\{MnV_{13}\}$ polyoxoanions, respectively.[10a,22] The bonds at 1495–1110 cm^{-1} are attributed to the DMF organic ligands. As seen in Figures S13–S14, the IR spectra of **2** and **3** exhibit similar characteristic peaks corresponding to compound **1**. The IR spectrum of **4** reveals a broad band located at 3354 and 3074 cm^{-1}, which can be assigned to the lattice and coordinated water molecules in the structure. The characteristic peaks at 979, 942, 825, 762, 653, 596 cm^{-1} can be attributed to ν (V═O) and ν (V–O–V) in the $\{MnV_{13}\}$ polyoxoanions, respectively (Figure S15). The peaks at 1589, 1385, 1283, and 1246 cm^{-1} are attributed to the isonicotinic acid molecule. The IR spectra of compounds **5** and **6** exhibit similar characteristic peaks corresponding to compound **7** (Figures S16–S17). The UV–vis spectra of compounds **1**–**6** were investigated with a 2 × 10^{-4} M concentration in aqueous solution. As shown in Figure S18 and S19, the absorbance at 257 and 264 nm in the ultraviolet region are attributed to the O → V charge transfer, respectively.[23]

TG Analysis. TG analyses of compounds **1**–**6** were carried out from 20 to 600 °C in order to estimate the thermal stability and the content of lattice–water molecules and organic ligands (Figures S20–S25). The TG curve of compound **1** reveals that the first weight loss is 7.51% in the temperature range from 20 to 88 °C, which corresponds to the release of lattice and coordinated water molecules in the structure (calcd. 7.34%). Then, two continuous weight loss steps of 19.37% occurred in the temperature range of 88–465 °C, mainly corresponding to the loss of the guest DMF and coordinated DMF molecules (calcd. 19.88%). The whole weight loss is 26.88%, in agreement with the theoretical weight loss value (calcd. 27.22%). In the DTA curve of **1**, the endothermic broad peak around 60 °C corresponds to the release of lattice and coordinated water molecules; The exothermic peaks at 474 °C is attributed to the decomposition of the polyoxoanion $[MnV_{13}O_{38}]^{7-}$. The TG curve of compound **2** and **3** exhibits two continuous weight loss stages in the temperature ranges 41–442 °C, corresponding to the loss of water molecules and DMF ligands. The whole weight loss is 21.54% for **2** and 23.23% for **3**, in agreement with the theoretical weight loss value (calcd. 20.25% for **2** and 25.50 for **3**).

The TG curve of compound **4** exhibits two continuous weight loss stages in the temperature range 54–495 °C. The first weight loss is 16.28% in the temperature range 54–318 °C, corresponding to the release of lattice and coordinated water molecules and free isonicotinic acid ligands in the framework (calcd. 17.24%). Then, the weight loss step of 14.83% occurred in the temperature range of 318–495 °C, mainly corresponding to the loss of the three coordinated isonicotinic acid molecules (calcd. 15.49%). The whole weight loss is 31.11%, in agreement with the theoretical weight loss value (calcd. 32.73%). The TG curve of compound **5** and **6** exhibit two continuous weight loss stages in the temperature range 37–494 °C, corresponding to the loss of water molecules and isonicotinic acid molecules. The whole weight loss is 32.64% for **5** and 23.90% for **6**, in agreement with the theoretical weight loss value (calcd. 32.68% for **5** and 23.14 for **6**).

CONCLUSIONS

In conclusion, six novel organic–inorganic compounds constructed of $\{MnV_{13}\}$ and rare earth metal–organic coordination units with 1D and 3D infinitely extended structures have been obtained. The successfully syntheses of the six complexes not only offered a series of attractive examples of structural topologies but also demonstrated an excellent precursor $\{MnV_{13}\}$ to construct POM-based organic–inorganic hybrid materials. Until now, the deliberate design of the POM-based organic–inorganic hybrids is still a challenge.

dx.doi.org/10.1021/cg500955d | Cryst. Growth Des. 2015, 15, 103–114

Therefore, reasonable design of the target compounds would generate a new method to obtain diverse structures.

■ ASSOCIATED CONTENT

Supporting Information

Single-crystal data of **1**−**6**, additional structural figures, characterizations including cyclic voltammograms, magnetic properties, IR, TG and UV−vis spectra. This material is available free of charge via the Internet at http://pubs.acs.org. Crystallographic data have been deposited at the Cambridge Crystallographic Data Center, CCDC reference number 1009719, 1009720, 1009721, 1009722, 1009723, and 1009724 for compounds **1**−**6**.

■ AUTHOR INFORMATION

Corresponding Authors

*(E.-B.W.) E-mail: wangeb889@nenu.edu.cn.

*(Y.L.) E-mail: luy968@nenu.edu.cn.

Notes

The authors declare no competing financial interest.

■ ACKNOWLEDGMENTS

This work was financially supported by the National Natural Science Foundation of China (No. 20901015), the Science and Technology Development Project Foundation of Jilin Province (No. 20130101006JC), the National Grand Fundamental Research 973 Program of China (2010CB635114).

■ REFERENCES

(1) (a) Lu, J.; Xu, Y.; K. Goh, N.; S. Chia, L. *Chem. Commun.* **1998**, 2733. (b) Fang, X. K.; Anderson, T. M.; Hill, C. L. *Angew. Chem., Int. Ed.* **2005**, *44*, 3540. (c) Xie, L.; Liu, S.; Gao, B.; Zhang, C.; Sun, C.; Li, D.; Su, Z. *Chem. Commun.* **2005**, 2402. (d) Dai, L.-M.; You, W.-S.; Li, Y.-G.; Wang, E.-B.; Huang, C.-Y. *Chem. Commun.* **2009**, 2721. (e) Li, C. R.; Li, S. Li.; Zhang, X. M. *Cryst. Growth Des.* **2009**, *9*, 1702. (f) Feng, J.; Zhang, H.-J. *Chem. Soc. Rev.* **2013**, *42*, 387.

(2) (a) Zhang, X.-M.; Hao, Z.-M.; Zhang, W.-X.; Chen, X.-M. *Angew. Chem., Int. Ed.* **2007**, *46*, 3456. (b) Tonigold, M.; Lu, Y.; Bredenkötter, B.; Rieger, B.; Bahnmüller, S.; Hitzbleck, J.; Langstein, G.; Volkmer, D. *Angew. Chem., Int. Ed.* **2009**, *48*, 7546. (c) Tong, X.-L.; Hu, T.-L.; Zhao, J.-P.; Wang, Y.-K.; Zhang, H.; Bu, X.-H. *Chem. Commun.* **2010**, *46*, 8543. (d) Lan, Y. Q.; Jiang, H. L.; Li, S. L.; Xu, Q. *Adv. Mater.* **2011**, *23*, 5015. (e) Liang, D.-D.; Liu, S.-X.; Ma, F.-J.; Wei, F.; Chen, Y.-G. *Adv. Synth. Catal.* **2011**, *353*, 733. (f) Wang, H.-N.; Meng, X.; Yang, G.-S.; Wang, X.-L.; Shao, K.-Z.; Su, Z.-M.; Wang, C.-G. *Chem. Commun.* **2011**, *47*, 7128.

(3) (a) Pope, M. T. *Heteropoly and Isopoly Oxometalates*; Springer: Berlin, 1983. (b) Müller, A.; Peters, F.; Pope, M. T.; Gatteschi, D. *Chem. Rev.* **1998**, *98*, 239. (c) Long, D. L.; Burkholder, E.; Cronin, L. *Chem. Rev.* **2007**, *36*, 105. (d) Li, Y. G.; Dai, L. M.; Wang, Y. H.; Wang, X. L.; Wang, E. B.; Su, Z. M.; Xu, L. *Chem. Commun.* **2007**, 2593. (e) Zhang, J.; Hao, J.; Wei, Y.; Xiao, F.; Yin, P.; Wang, L. *J. Am. Chem. Soc.* **2009**, *132*, 14. (f) Dolbecq, A.; Dumas, E.; Mayer, C. R.; Mialane, P. *Chem. Rev.* **2010**, *110*, 6009. (g) Liu, T.; Langston, M. L.; Li, D.; Pigga, J. M.; Pichon, C.; Todea, A. M.; Muller, A. *Science* **2011**, *331*, 1590. (h) Miras, H. N.; Yan, J.; Long, D.-L.; Cronin, L. *Chem. Soc.Rev.* **2012**, *41*, 7403. (i) Yin, P.; Zhang, J.; Li, T.; Zuo, X. B.; Hao, J.; Warner, A. M.; Chattopadhyay, S.; Shibata, T.; Wei, Y. G.; Liu, T. B. *J. Am. Chem. Soc.* **2013**, *135*, 4529.

(4) (a) Zheng, S. T.; Zhang, J.; Yang, G. Y. *Angew. Chem., Int. Ed.* **2008**, *47*, 3909. (b) Li, J.; Huth, I.; Chamoreau, L.-M.; Hasenknopf, B.; Lacôe, E.; Thorimbert, S.; Malacria, M. *Angew. Chem., Int. Ed.* **2009**, *48*, 2035.

(5) (a) Du, D.-Y.; Qin, J.-S.; Wang, T.-T.; Li, S.-L.; Su, Z.-M.; Shao, K.-Z.; Lan, Y.-Q.; Wang, X.-L.; Wang, E.-B. *Chem. Sci.* **2012**, *3*, 705. (b) Yin, P.; Wang, J.; Xiao, Z.; Wu, P.; Wei, Y.; Liu, T. *Chem.—Eur. J.* **2012**, *18*, 9174.

(6) (a) Niu, J.-Y.; Guo, D.-J.; Wang, J.-P.; Zhao, J.-W. *Cryst. Growth Des.* **2004**, *4*, 241. (b) Dolbecq, A.; Mialane, P.; Lisnard, L.; Marrot, J.; Sécheresse, F. *Chem.—Eur. J.* **2003**, *9*, 2914. (c) An, H. Y.; Li, Y. G.; Xiao, D. R.; Wang, E. B.; Sun, C. Y. *Cryst. Growth Des.* **2006**, *6*, 1107. (d) Liu, C.; Luo, F.; Liu, N.; Cui, Y.; Wang, X.; Wang, E. B.; Chen, J. *Cryst. Growth Des.* **2006**, *6*, 2658. (e) Song, Y.-F.; Long, D.-L.; Kelly, S. E.; Cronin, L. *Inorg. Chem.* **2008**, *47*, 9137. (f) Liu, D.; Tan, H.-Q.; Chen, W.-L.; Li, Y.-G.; Wang, E.-B. *CrystEngComm* **2010**, *12*, 2044. (g) An, H.; Han, Z.; Xu, T. *Inorg. Chem.* **2010**, *49*, 11403. (h) Han, Q.; He, C.; Zhao, M.; Qi, B.; Niu, J.; Duan, C. *J. Am. Chem. Soc.* **2013**, *135*, 10186.

(7) Miras, H. N.; Wilson, E. F.; Cronin, L. *Chem. Commun.* **2009**, 1297.

(8) (a) Zou, C.; Zhang, Z.; Xu, X.; Gong, Q.; Li, J.; Wu, C.-D. *J. Am. Chem. Soc.* **2011**, *134*, 87. (b) Zheng, S.-T.; Zhang, J.; Li, X.-X.; Fang, W.-H.; Yang, G.-Y. *J. Am. Chem. Soc.* **2010**, *132*, 15102.

(9) Liu, S. X.; Li, D. H.; Xie, L. H.; Cheng, H.; Zhao, X.; Su, Z. *Inorg. Chem.* **2006**, *45*, 8036.

(10) (a) Flynn, C. M.; Pope, M. T. *J. Am. Chem. Soc.* **1969**, *92*, 85. (b) Li, D. H.; Liu, S. X.; Sun, C. Y.; Xie, L. H.; Wang, E. B.; Hu, N. H.; Jia, H. Q. *Inorg. Chem. Commun.* **2005**, *8*, 433.

(11) (a) Tatsuno, Y.; Nakamura, C.; Saito, T. *J. Mol. Catal.* **1987**, *42*, 57. (b) Fukuda, N.; Yamase, T. *Biol. Pharm. Bull.* **1997**, *20*, 927.

(12) Liu, D.; Lu, Y.; Tan, H.-Q.; Chen, W.-L.; Zhang, Z.-M.; Li, Y.-G.; Wang, E.-B. *Chem. Commun.* **2013**, *49*, 3673.

(13) (a) Sheldrick, G. M. *SHELXS97, Program for Crystal Structure Refinement*; University of Göttingen: Göttingen, Germany, 1997. (b) Sheldrick, G. M. *SHELXS97, Program for Crystal Structure Solution*; University of Göttingen: Göttingen, Germany, 1997.

(14) (a) Roy, S. *CrystEngComm* **2014**, *16*, 4667. (b) Roy, S. *Comment Inorg. Chem.* **2011**, *32*, 113.

(15) An, H.; Li, Y.; Wang, E.; Xiao, D.; Sun, C.; Xu, L. *Inorg. Chem.* **2005**, *44*, 6062.

(16) (a) Jia, L.-N.; Hou, L.; Wei, L.; Jing, X.-J.; Liu, B.; Wang, Y.-Y.; Shi, Q.-Z. *Cryst. Growth Des.* **2013**, *13*, 1570−1576. (b) Xu, W.; Zhou, Y.; Huang, D.; Xiong, W.; Su, M.; Wang, K.; Han, S.; Hong, M. *Inorg. Chem.* **2011**, *50*, 8437−8451. (c) Lu, Y.-B.; Jian, F.-M.; Jin, S.; Zhao, J.-W.; Xie, Y.-R.; Luo, G.-T. *Cryst. Growth Des.* **2014**, *14*, 1684−1694.

(17) (a) An, H. Y.; Han, Z. B.; Xu, T. Q. *Inorg. Chem.* **2010**, *49*, 11403. (b) Qin, C.; Song, X. Z.; Su, S. Q.; Dang, S.; Feng, J.; Song, S. Y.; Hao, Z. M.; Zhang, H. J. *Dalton Trans.* **2012**, *41*, 2399. (c) Zhang, D.; Lu, Y.; Chen, L.; Cai, H.; Zhu, D.; Xu, Y. *CrystEngComm* **2012**, *14*, 6627.

(18) (a) Fang, X.; Kogerler, P. *Chem. Commun.* **2008**, 3396. (b) Li, Y.-W.; Li, Y.-G.; Wang, Y.-H.; Feng, X.-J.; Lu, Y.; Wang, E.-B. *Inorg. Chem.* **2009**, *48*, 6452.

(19) (a) Li, C.; Zhang, Y.; O'Halloran, K. P.; Zhang, J.; Ma, H. *J. Appl. Electrochem.* **2008**, *39*, 421. (b) Bi, L.-H.; Kortz, U.; Dickman, M. H.; Nellutla, S.; Dalal, N. S.; Keita, B.; Nadjo, L.; Prinz, M.; Neumann, M. *J. Cluster Sci.* **2006**, *17*, 143.

(20) (a) Camp, T. R. *Water and Its Impurities*; Reinhold Pub. Corp.: New York, 1963. (b) Metzler, D. E. *Biochemistry: The Chemical Reactions of Living Cells*; Academic Press: New York, 1977. (c) Belhouari, A. B. K; Nadjo, L.; Contant, R. *New J. Chem.* **1998**, *22*, 83. (d) Bassil, B. S.; Kortz, U.; Tigan, J. M.; Keita, B.; Nadjo, L. *Inorg. Chem.* **2005**, *44*, 9360.

(21) (a) McCormac, T. D. F.; Drennan, D. G. *Electroanalysis* **2001**, *13*, 836. (b) Wang, X. L.; Kang, Z. H.; Wang, E. B.; Hu, C. W. *J. Electroanal. Chem.* **2002**, *523*, 142. (c) Li, L. D.; Li, W. J.; Sun, C. Q.; Li, L. S. *Electroanalysis* **2002**, *14*, 368.

(22) Lan, Q.; Tan, H.; Liu, D.; Wang, E. *J. Solid State Chem.* **2013**, *199*, 129.

(23) Wu, Q.; Hao, X.; Feng, X.; Wang, Y.; Li, Y.; Wang, E.; Zhu, X.; Pan, X. *Inorg. Chem. Commun.* **2012**, *22*, 137.